Journal Pre-proofs

Ultrafast, Scalable and Green Synthesis of Amorphous Iron-Nickel based Durable Water Oxidation Electrode with Very High Intrinsic Activity via Potential Pulses

Shiyu Liu, Guodong Han, Jian Zhang, Hao Wang, Xiaoxi Huang

PII: S1385-8947(21)02274-9
DOI: https://doi.org/10.1016/j.cej.2021.130688
Reference: CEJ 130688

To appear in: *Chemical Engineering Journal*

Received Date: 11 February 2021
Revised Date: 28 May 2021
Accepted Date: 2 June 2021

Please cite this article as: S. Liu, G. Han, J. Zhang, H. Wang, X. Huang, Ultrafast, Scalable and Green Synthesis of Amorphous Iron-Nickel based Durable Water Oxidation Electrode with Very High Intrinsic Activity via Potential Pulses, *Chemical Engineering Journal* (2021), doi: https://doi.org/10.1016/j.cej.2021.130688

Ultrafast, Scalable and Green Synthesis of Amorphous Iron-Nickel based Durable Water Oxidation Electrode with Very High Intrinsic Activity via Potential Pulses

Shiyu Liu,[1] Guodong Han,[1] Jian Zhang[1,2] Hao Wang[1] and Xiaoxi Huang[1]*

[1]Hoffmann Institute of Advanced Materials, Postdoctoral Innovation Practice Base, Shenzhen Polytechnic. 7098 Liuxian Blvd, Nanshan District, Shenzhen, 518055, PR China.

[2]School of Chemistry and Chemical Engineering, South China University of Technology. Guangzhou 510640, PR China.

Corresponsence and requests for materials should be addressed to X. H. (E-mail: xiaoxihuang@szpt.edu.cn)

KEYWORDS: oxygen evolution reaction, pulsed synthesis, electrocatalyst, iron, water splitting

ABSTRACT. Electrochemical water splitting to produce clean hydrogen fuel provides a route to store electrical energy based on intermittent renewable energy sources. Oxygen evolution reaction (OER) is an essential reaction in water splitting process and requires efficient electrocatalyst to lower the overpotential. However, current electrocatalysts are limited by the complicated synthetic protocols, especially long synthesis time, along with poor intrinsic catalytic activity. Here we report a low-cost and scalable electrochemical method to synthesize efficient water oxidation electrode via potential pulses. In a two-electrode setup, two water oxidation electrodes are synthesized in merely 10 s. These two electrodes need overpotentials of 240.7±6.8 mV and 239.5±3.4 mV to catalyze OER at 10 mA/cm^2 current density normalized by geometric area. Remarkably, when normalized by electrochemically active surface area, the intrinsic catalytic activity outperformed the state-of-the-art catalysts. And the electrode is durable to catalyze OER at 100 mA/cm^2, even after repeated ultrasonication treatment, the overpotential only shift 25 to 51 mV. We postulate that the highly disordered defective sites of nickel hydroxide modified with iron species are the most active OER catalytic sites. In addition, The attempt to synthesize 10 water oxidation electrodes using this concept is very successful, further reducing the cycle time to 1 s per electrode. The super facile synthesis procedures, as well as the excellent catalytic performance make these materials highly suitable for large scale applications.

1. Introduction

Searching for suitable materials to drive electrochemical water splitting process under low overpotential is a very hot research topic in recent years, especially the materials that can catalyze sluggish oxygen evolution reaction (OER).[1-8] To achieve economic feasibility of the electrochemical water splitting process, not only the activity and stability of catalysts must be high enough, but also the synthesis strategies matter.[9-11] In terms of the method to synthesize water oxidation electrode, it must at least satisfy the following criteria: fast, facile, scalable and environmentally friendly. Among these factors, the synthesis time used to fabricate the catalyst is of essential importance as it can influence the production efficiency and determine the applicability of synthetic method for practical applications. Reducing the synthesis time of the overall synthetic process can not only improve the productivity, but also reduce the cost.

Because of the importance of reducing synthesis time, a growing attention is being paid on developing ultrafast strategies. Various methods of preparation, including but not limited to microwave assisted method, solution based chemical treatment, thermal treatment, electrochemical method, were reported to synthesize OER electrocatalysts in relatively short time. For example, Xu *et al.* reported a method to convert metal organic framework (MOF)/graphene into (FeNiP)/P-doped graphene composites via microwave assisted thermal treatment in 20 s. But the synthesis of MOF/graphene precursor still required multiple steps and quite a long time.[12] Regarding to the solution based chemical treatment, Zou *et al.* found that amorphous NiFe bimetallic hydroxide films can be coated on Ni_3S_2 nanosheets supported on nickel foam in 5 s at 100 °C, but it's a two step process and the first step also required 5 h hydrothermal reaction in an autoclave to grow Ni_3S_2 nanosheets on the surface of nickel foam.[13] Recently, an ultrafast protocol is reported to synthesize S-doped NiFe (oxy)hydroxide in 5 min at room temperature for alkaline seawater splitting.[14] The synthesis involves the immersion of nickel foam into the solution of $Fe(NO_3)_3 \cdot 9H_2O$ and $Na_2S_2O_3 \cdot 5H_2O$ for 5 min.

Another method was reported to synthesize amorphous NiFe nanosheets on iron foam by addition of cleaned iron foam into the solution of H_2O_2/$Ni(NO_3)_2$/$Fe(NO_3)_3$ for 200 s.[15] High temperature can generally accelerate the formation of catalytic active materials, for instance, a mercaptoethanol solution was dropped directly on nickel foam, followed by annealing at 300 °C for 50 s to synthesize nickel sulfide film on nickel foam for overall electrochemical water splitting. The resulting catalyst can catalyze OER at a current density of 10 mA/cm^2 with 312 mV overpotential.[16] In another example, Hu *et al.* reported a method to synthesize CoS/graphene composite material by high temperature treatment at ca. 2000 K in milliseconds for overall water splitting, however, there are several steps required prior to the thermal shock treatment.[17] Electrochemical methods, featured with the merits of fast and simple setup, have great potential to decrease the synthesis time. For example, NiFe layered double hydroxide can be synthesized on nickel foam via electrodeposition in 300 s.[18] Another pulsed electrodeposition method was reported by using sequential 2 s cathodic current pulses at -10 mA/cm^2 for 2 to 20 cycles, and there's 10 s stirring between each pulse.[19] However, these methods are both expensive - involving high cost reagents - and / or time consuming to synthesize.

Reducing the synthesis time is advantageous to lower the cost of materials used to fabricate the water electrolyzer, and this is one-time capital cost. To make sure the electrolyzer can run on small operating cost, the electrocatalyst must be capable to drive high catalytic current density at low overpotential. Both of these two factors are of equal importance. We summarized the synthesis time and the overpotential required to catalyze 10 mA/cm^2 current density of some representative materials in Fig. 1. As we can see, most of the reported catalysts fail either one of the criteria. The challenge to synthesize materials in very short time while maintaining their high

catalytic activity is still immense. Therefore, it's urgent to develop novel method to synthesize water oxidation electrodes that can satisfy both requirements.

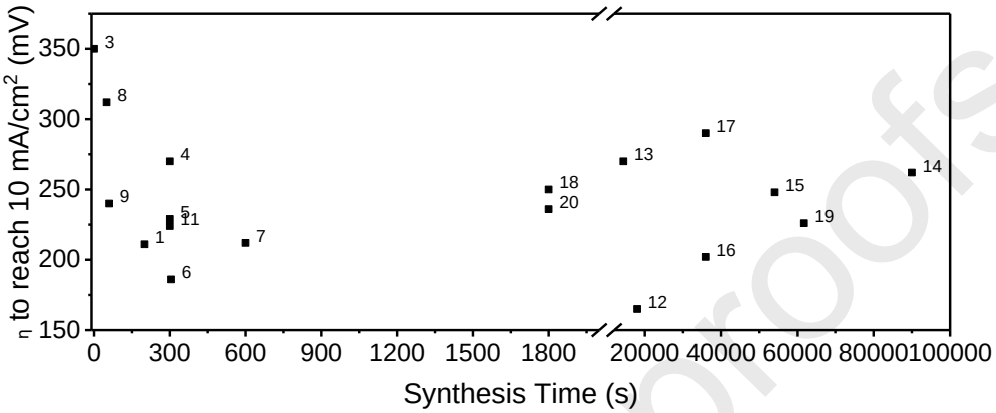

Fig. 1. Comparison of overpotential required to catalyze 10 mA/cm^2 OER current density and the synthesis time for different reported OER electrocatalysts: 1-amorphous NiFe on iron foam;[15] 2-Cu oxides micro/nano-structures;[20] 3-CoS@few-layer graphene;[17] 4-NiCo-LDH on stainless steel mesh;[21] 5-S-doped Ni/Fe (oxy)hydroxide on nickel foam;[14] 6-amorphous NiFe metal oxyhydroxide on nickel foam;[22] 7-amorphous Fe-Co-Ni hydroxide on nickel foam;[23] 8-Ni_3S_2 films on nickel foam;[16] 9-NiFe LDH on nickel foam;[24] 10-NiFeP/graphene heterostructure;[12] 11-NiFe LDH on nickel foam;[18] 12-amorphous NiFe hydroxide on Ni_3S_2;[13] 13-boronized NiFe alloy sheet;[25] 14-NiCo LDH on CuO nanowires;[26] 15-CoFeCr nanosheet on nickel foam;[27] 16-Co-doped FeNi carbonate hydroxide on nickel foam;[28] 17-tannin NiFe complex film on carbon fiber paper;[29] 18-Ag@Co(OH)x;[30] 19-hexagonal close - packed NiFe@N-doped carbon;[31] 20-FeNiRedox.[32] All of the OER evaluations were performed in 1.0 M KOH.

In our previous report, we have demonstrated that iron plate after consecutive oxidation and reduction process in $NiSO_4$ electrolyte via cyclic voltammetry (CV) potential cycling can lead to

highly active water oxidation electrode.[32] But the potential cycling method takes as long as 30 min, still far away from our expectation. In order to address the aforementioned challenges, we present an ultrafast (10 s), scalable and green electrochemical method to synthesize amorphous water oxidation electrodes by applying pulsed potentials between two iron plates in an aqueous $NiSO_4$ solution. The synthesis process in a two-electrode cell is systematically studied. The obtained two iron-based water oxidation electrodes can catalyze OER at 10 mA/cm^2 geometric current density at the overpotential of 240.7±6.8 mV and 239.5±3.4 mV, respectively. Because the synthesis time is very short, after the deposition of nickel hydroxide, there's no sufficient time for iron to fully diffuse into the lattice of nickel hydroxide, instead, iron prefer to incorporate at the defected sites or edge sites, which actually endow the materials with higher catalytic activity. Considering both catalytic performance and fabrication time, our catalyst outweighs previously reported catalysts. Additionally, we constructed a ten-electrode setup to demonstrate that the design can be used to synthesize ten water oxidation electrodes in 10 s. This work provides important insights on ultrafast synthesis of active electrodes for various electrochemical applications.

2. Experimental Section

2.1. Solution Preparation

18.2 MΩ•cm water, supplied by Aquaplore, was used to prepare solutions. A stock solution of 0.1 M $NiSO_4•6H_2O$ (99.9% metals basis, Shanghai Aladdin Biochemical Co., Ltd.) was prepared as the electrolyte to synthesize water oxidation electrodes. A solution of 0.05 M $Fe_2(SO_4)_3$ (AR, Fe 21-23%, Shanghai Macklin Biochemical Co., Ltd) was prepared. Another solution of 1 M KOH (99.99% metals basis, Shanghai Aladdin Biochemical Co., Ltd.) was prepared to evaluate the electrocatalytic OER activity.

2.2. Pulsed Potential Synthesis

A fine sandpaper (3M) was used to polish the surface of iron plate (thickness: 0.3 mm, Qinghe Guantai Metal Materials Co., Ltd.), and ethanol was used to clean the surface by ultrasonication. Afterwards, the cleaned iron plate was cut into strips (size: 0.5 cm × 5 cm) and covered with hot melt glue to expose ca. 0.2 cm^2 area for immersion into the electrolyte.

For the two-electrode setup, two identical iron plates were placed in parallel in 0.1 M $NiSO_4$ solution, one of the iron plates was connected with the banana plugs of WE and sensing electrode (SE), the other iron plate was connected with the banana plugs of RE and CE (Fig. 2a). A pulsed potential program was applied between two electrodes. The potential value started at +2.4 V for 5 s and changed to -2.4 V for another 5 s. After 10 s synthesis, both electrodes were taken out of the solution and cleaned by ultrapure water. Depending on which banana plugs they connected, the as-synthesized electrodes were named as IronWE and IronCE, respectively. In addition to above mentioned synthetic condition, the synthesis was performed under other different potential values and times to get more insights of this method. The synthesis was performed in the temperature range of 25±1 ℃.

A scalable fabrication setup is shown in Fig. S1, several pairs of iron strips were placed in parallel, half of them were connected with the banana plugs of WE and SE cables and the other iron plates were connected with RE and CE cables. The same pulsed potential program of ±2.4 V was used for the synthesis in 10 s.

2.3. Electrode Characterizations

The surface of electrode was observed by a field emission scanning electron microscope (SEM) (Hitachi, SU 8220). The total nickel content after pulsed synthesis was probed by inductively coupled plasma atomic emission spectroscopy (ICP-OES) (Agilent 720ES). X-ray diffraction patterns were measured on a Bruker D8 Advance diffractometer. The surface compositions of electrodes were measured by X-ray photoelectron spectroscopy (XPS) (Thermo Fisher Scientific K-Alpha, with mono Al Kα). The peak of C 1s (at 284.8 eV) corresponding to adventitious carbon was used to calibrate the energy scale.

2.4. Electrochemical Measurements

The OER catalytic activities of the as-synthesized iron-based electrodes were evaluated by using a PARSTAT MC electrochemical workstation (Princeton Applied Research) in a three-electrode cell, in which the Hg/HgO electrode, graphitic carbon rod, as-synthesized electrode served as RE, CE and WE, respectively. All electrochemical measurement was conducted at room temperature (25±1°C). Cyclic voltammetry (CV) curves were measured at a scan rate of 10 mV/s. Linear sweep voltammetry (LSV) plots were recorded at a lower scan rate of 1 mV/s to minimize the effect of capacitive current. The equation below was used to convert the measured potential to RHE scale and compensate the system resistance:

$$E_{\mathrm{RHE}} = E_{\mathrm{Hg/HgO}} + 0.925\ \mathrm{V} - 85\% \times i \times \mathrm{Rs} \qquad (1)$$

where –0.925 V is the potential found at zero current value during the calibration of Hg/HgO RE,[32] i is the recorded current (A) and Rs is system resistance (Ω), which was determined by the AC impedance data. AC impedance data was collected at a potential of

1.5 V vs. RHE by using the following parameters: start frequency = 10^4 Hz; end frequency = 10^{-2} Hz; amplitude = 5 mV. The range of Rs was 1.8-3.5 Ω in this report.

To compare the catalytic activity, geometric current density was calculated by normalizing the measured current with geometric surface area.

2.5. Electrochemically Active Ni Sites

The amount of electrochemically active Ni sites can be determined by integration of the Ni reduction peak in CV curves. An example is shown in Fig. S1. The following equation is used to calculate the loading of active Ni amount on the surface:

$$\text{Active Ni} = Q / (A \times m \times F) \qquad (2)$$

where Q equals the charges for Ni reduction peak, A is the geometric area of the electrode, m is the number of electrons transferred to reduction one nickel cation and it's assumed as 1 in this paper, F is Faraday constant (96485 C/mol).

2.6. Double Layer Capacitance

The double layer capacitance (C_{dl}) was measured by recording the CV curves at a series of scan rates (0.1, 0.08, 0.06, 0.04, 0.02 and 0.01 V/s) in a non-Faradaic potential window from 0.1 to 0.3 V vs. Hg/HgO in 1 M KOH. Half of the differences of anodic and cathodic current values (mA) at 0.2 V vs. Hg/HgO were plotted against the scan rates (V/s). The resulting slope of the fitted line was C_{dl}. The electrochemical active surface area (ECSA) was calculated according to the following equation:

$$\text{ECSA} = C_{dl} / (0.04\ \text{mF/cm}^2) \qquad (3)$$

where 0.04 mF/cm^2 represent the specific capacitance of the materials.[26] The intrinsic catalytic activity or specific activity was calculated by normalizing the measured current with ECSA.

The C_{dl} density, normalized by the geometric area of the electrode, was calculated based on the following equation:

$$C_{dl}\ \text{density} = C_{dl} / A \qquad (4)$$

where A represents the geometric area of the electrode. The C_{dl} density is related with the effective ECSA and can be used to compare the effective surface area or roughness factor of each electrode.

2.7. Turnover Frequency (TOF) Calculations

The following equation was used to calculate the TOF:

$$TOF = i / (4 \times F \times n) \qquad (5)$$

where i is the current recorded during the OER, 4 is the number of electrons required to produce one oxygen molecule, F is the Faraday constant (96485 C/mol), and n is the number of active sites (mol) in the catalysts.[33] Two different strategies were used to determine n. For the first one, total nickel content was probed by ICP-OES, and iron amount was calculated based on nickel/iron atomic ratios measured by XPS. The calculation will yield TOF_{all} because it's under the assumption that all the deposited nickel and iron are the active sites. However, this could underestimate the intrinsic catalytic activity because some deeply buried atoms are not accessible to the electrolyte. Another method was only based surface nickel/iron sites, where nickel content was derived from the Ni^{2+}/Ni^{3+} reduction peak in the CV by assuming one electron transfer

per nickel, and iron amount was still deduced from nickel/iron atomic ratios. This will result in $TOF_{surface}$ as only electrochemically accessible surface nickel+iron sites were considered as active centers.

3. Results and Discussion

3.1. Electrode Synthesis and Structural Properties

Detailed experimental procedures are described in experimental section. In a two-electrode setup as shown in Fig. 2a, iron strips and $NiSO_4$ solution together construct an electrolyzer, in which the oxidation reactions and reduction reactions proceed at the same time but on different locations, namely, anode and cathode. Anodic current is observed when the applied voltage was +2.4 V (Fig. 2b), indicating that oxidation reaction happened on IronWE, which could be associated with the oxidation of iron to iron species with high oxidation number. Concurrently, the reduction reaction must happen on IronCE. This is further verified by the observation of gas bubbles on IronCE due to hydrogen evolution reaction (HER). The Ni^{2+} in the electrolyte can react with OH^- generated from HER, producing nickel hydroxide on the surface of iron. As the voltage changes to -2.4 V, cathodic current is recorded because reduction reaction happens on IronWE and also proved by the rapidly evolved hydrogen bubbles. Besides HER, the reduction of highly oxidative iron species may contribute to some cathodic charges. Meanwhile, oxidation reaction should happen on IronCE, and the produced Fe^{2+}/Fe^{3+} can easily be doped into nickel hydroxide structure. These major reactions are illustrated in Fig. 2a. To study the influence of these two voltage segments, two additional electrodes, namely, IronWE5s and IronCE5s, were synthesized by applying +2.4 V between two iron strips for 5s (Fig. 2c). During this time, oxidation reaction happens on IronWE and reduction reaction happens on IronCE.

After the synthesis, CV curves were recorded in 1 M KOH electrolyte at 10 mV/s to quickly check the nickel content on the surface by integrating the reduction peak area of Ni^{2+}/Ni^{3+} and assume that the reduction is one electron process (Fig. S1).[34] After first 5 s, the electrochemically accessible Ni is 0.12 ± 0.05 μmol/cm^2 for IronWE5s, significantly lower than that of 1.07 ± 0.35 μmol/cm^2 on IronCE5s. This means the primary reaction on IronCE is nickel hydroxide cathodic deposition in the first 5 s, whereas small amount of Ni^{2+} from the electrolyte can also be trapped on the surface of IronWE during this period. After additional 5 s at -2.4 V, IronWE10s and IronCE10s have close surface nickel content of 0.69 ± 0.19 and 0.86 ± 0.14 μmol/cm^2, respectively, indicating that nickel hydroxide is deposited on the surface of IronWE in the second 5 s period.

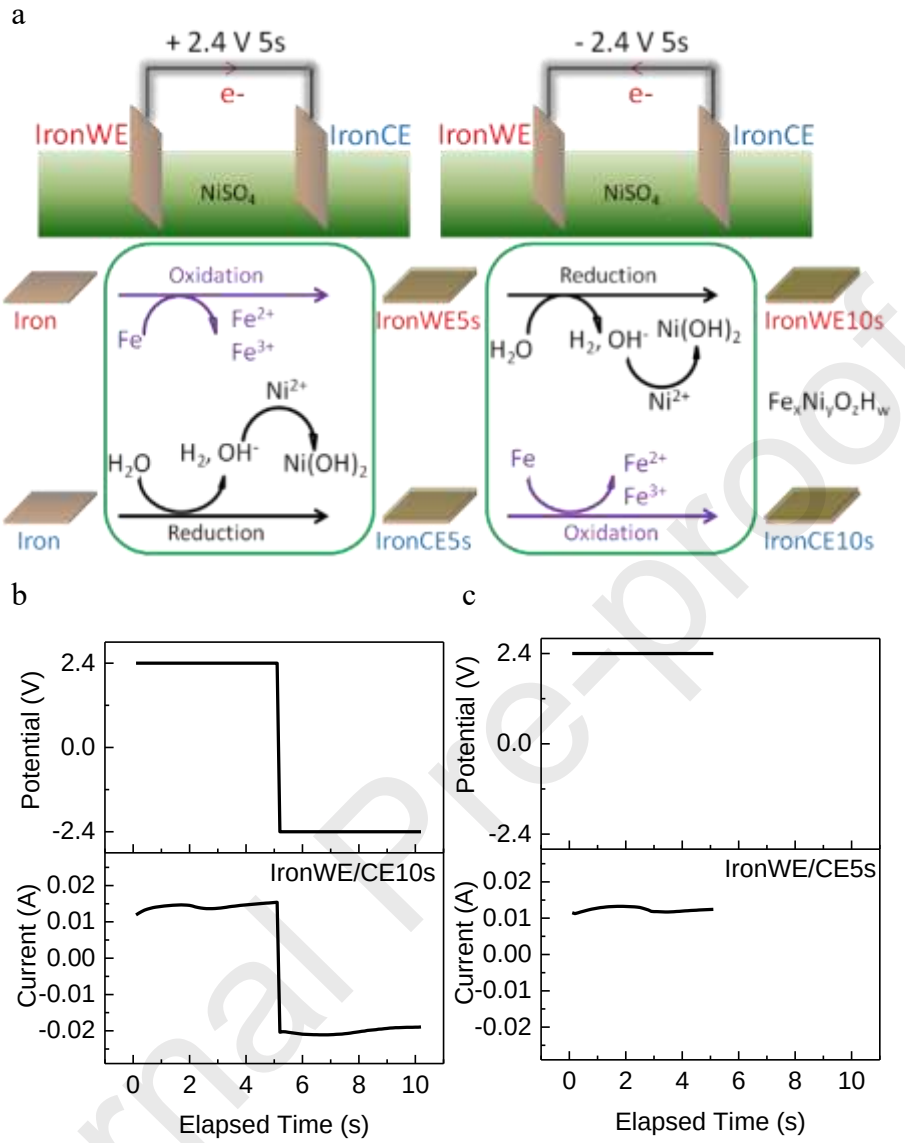

Fig. 2. (a) A two-electrode setup used to synthesize two water oxidation electrodes at the same time and the proposed electrochemical reactions on the surface of iron during the pulsed potential treatment. The recurrent potential pulses (top) applied between two iron strips to synthesize (b) IronWE/CE10s, (c) IronWE/CE5s and the corresponding current *versus* elapsed time curve (bottom).

To further study the chemical composition and local structure of these four electrodes, X-ray photoelectron spectroscopy (XPS) measurements were performed. The core-level spectra of Ni 2p (Fig. 3a) confirm that all of the surfaces are composed of Ni(II) bonded with hydroxide species, as evidenced by the characteristic peaks at binding energies of 855.5 eV (Ni $2p_{3/2}$) and 873.3 eV (Ni $2p_{1/2}$).[35] In terms of the Fe 2p XPS spectra (Fig. 3b), the Fe $2p_{3/2}$ signal of IronWE5s is located at lower binding energy of 710.3 eV, compared with 712.2 eV for other three electrodes. This means that most of the Fe(III) species in IronWE5s exist in oxide form, while Fe(III) primarily bind with hydroxides in the electrode of IronCE5s, IronWE10s and IronCE10s.[35] This conclusion is further proved by the O 1s XPS spectra. As shown in Fig. 3c, only IronWE5s displays a shoulder peak at 529.6 eV due to the presence of metal-oxygen bond, whereas other three electrodes exhibit a single peak at 531.2 eV corresponding to the metal-hydroxide moiety.[36, 37] It should be noted that even IronCE5s has only experienced cathodic reduction process, it also contains 11% of Fe(III) based on XPS analysis (Fig. 3d). With the iron plate serving as the substrate, we believe doping of iron into nickel hydroxide is inevitable under such condition, possibly due to the corrosion process.[26] Moreover, in terms of IronWE5s, the electrochemical oxidation of iron can produce Fe^{2+} cation, which could further be oxidized electrochemically or chemically to Fe^{3+}, in the latter case, dissolved molecular oxygen serves as oxidant ($O_2 + 2H_2O + 4e^- = 4OH^-$) and generates a locally high alkaline environment. Ni^{2+} from the electrolyte can be precipitated in such condition. But IronWE5s still has the lowest amount of nickel compared with other three electrodes, this further confirms that nickel hydroxides predominantly come from cathodic deposition. In summary, a general formula of $Fe_xNi_yO_zH_w$ can be used to describe the composition of surface coating after pulsed synthesis.

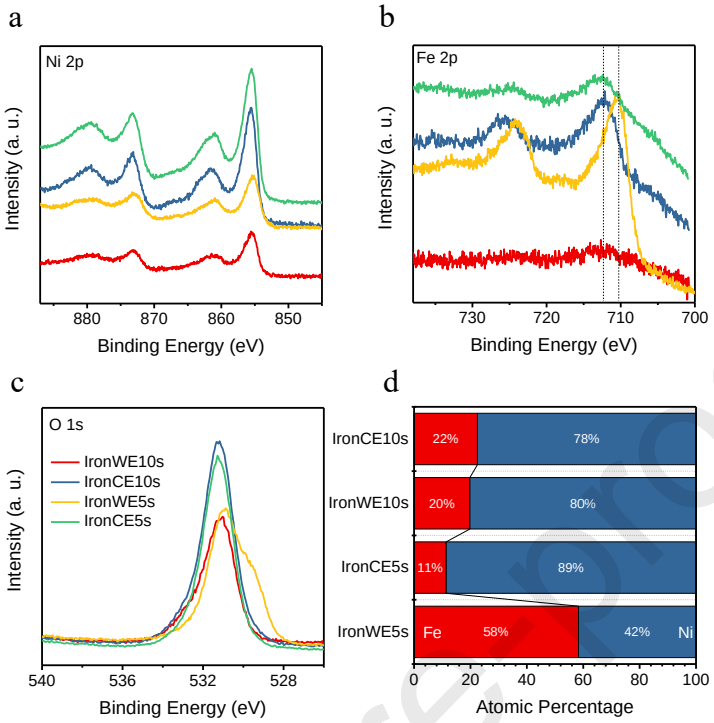

Fig. 3. High resolution XPS spectra of (a) Ni 2p, (b) Fe 2p and (c) O 1s for IronWE10s, IronCE10s, IronWE5s and IronCE5s. (d) Atomic percentage of iron and nickel based on XPS measurements.IronWE

The morphologies of iron electrodes after pulsed synthesis were identified with scanning electron microscopy (SEM) and the results are displayed in Fig. S2 and Fig. 4. After first 5 s, both IronWE5s and IronCE5s electrodes show nanosheet morphology. After the next 5 s, there are many additional nanoflower particles on IronWE10s, the nanoflower particles are also constructed by nanosheets. The Energy Dispersive Spectrometer (EDS) mappings indicate that nickel elements are primarily distributed at the nanoflower sites, suggesting that these nanoflowers are produced during second 5 s and associated with the cathodic electrodeposition of nickel hydroxide. In terms of IronCE10s, it still predominantly contains nanosheets, but several round areas with clear boundaries are observed on the surface. The nonuniformity of

electrodes synthesized after 10 s is because they were treated under two different potential values, which triggered reduction and oxidation reactions separately.

To get further insights about surface dynamic change during the pulsed potential synthesis, an optical microscope is used to observe the surface of iron plate. The setup is shown in Fig. S3 and the optical images of iron plate during the synthesis are shown in Fig. S4. For IronWE10s, in the first 5 s, the surface becomes rougher and new structures appear with different contrast, this could be related with iron oxidation, in the next 5 s, some of the structure motifs disappear, which may due to the reduction of oxidized iron species, but some still retain, indicating that new films are coated on the surface. In terms of the IronCE10s, in the first potential loop, new structures quickly evolve on the surface, this is related with the electrodeposited of nickel hydroxide as well as the HER process. In the subsequent potential loop, this structure preserves. Because of the resolution limit for optical microscope, it's difficult to look at detailed structures in nanoscale resolution. However, in combination with SEM images, these results at least prove that the formation or generation of new coatings on iron surface is very fast.

3.2. Evaluation of OER Performance and Intrinsic Activity

The electrocatalytic activities of the above synthesized electrodes towards OER were evaluated in 1 M KOH solution. The catalytic performance described by the current density normalized by geometric area is shown in Fig. 5a and 5b. IronWE5s has the lowest catalytic activity, giving much higher overpotential of 273.2 ± 11.7 mV to drive 10 mA/cm^2 current density. This could be ascribed to the lowest nickel content on the surface as discussed above. IronCE5s has enhanced catalytic activity and the overpotential is reduced to 241.5 ± 4.3 mV, this value is approaching the performance of IronWE10s and IronCE10s, which reveal the overpotential of 240.7±6.8 mV and 239.5±3.4 mV to reach the same 10 mA/cm^2 current density. These results indicate that the

novel pulsed potential method using two-electrode design can be used to synthesize very active water oxidation electrodes in very short time, namely 5 s per electrode, which successfully meet both criteria of high activity + ultrafast.

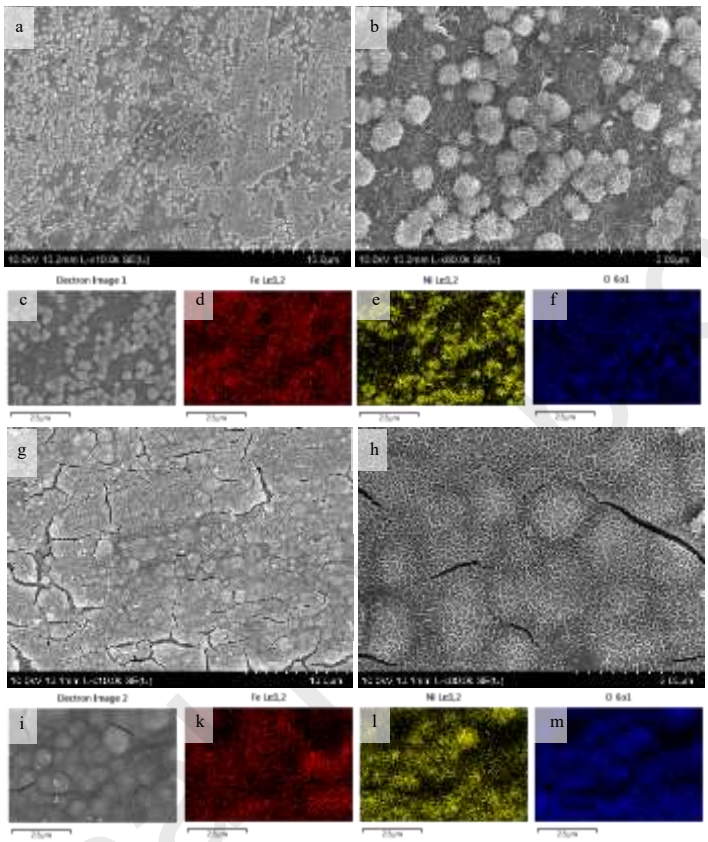

Fig. 4. (a) Low magnification and (b) high magnification SEM images of IronWE10s. (c) The electron microscope image of IronWE10s used for elemental mapping and the corresponding mapping for (d) iron, (e) nickel and (f) oxygen. (g) Low magnification and (h) high magnification SEM images of IronCE10s. (i) The electron microscope image of IronCE10s used for elemental mapping and the corresponding mapping for (j) iron, (k) nickel and (l) oxygen.

For comparison purpose, electrodes synthesized with longer time of 60 s and 360 s were prepared by conducting the potential pulses for 6 and 36 loops. As shown in Fig. S5, repeated

anodic and cathodic current was observed during the synthesis, suggesting that oxidation/reduction reactions happened on the surface alternatively. The resulting electrodes are named as IronWE60s, IronCE60s, IronWE360s and IronCE360s, respectively. Extending the synthesis time significantly increases the electrochemical active surface area (ECSA), which is evidenced by the trending up of C_{dl} density (Fig. S6 and S7). Aside from ECSA, the catalyst loading also increases, for example, according to Inductively Coupled Plasma Optical Emission Spectroscopy (ICP-OES) analysis, the total nickel content for IronCE10s, IronCE60s and IronCE360s are 1.89, 3.21 and 8.28 μmol/cm^2. It's generally accepted that increasing the catalyst

loading can increase the geometric current density, and improving ECSA can also lead to high catalytic activity because the electrode can expose more active sites for catalysis.[38, 39] However, from 10 s, to 60 and 360 s, the overpotential values required to reach 10 mA/cm^2 geometric current density are close with each other regardless of the increasing of catalyst loading and ECSA, suggesting that there are some other key parameters that determine the catalytic activity (Fig. 5a and 5b). The current density normalized by ECSA can avoid the impact of catalysts' surface area on the catalytic performance and it's one of the strategies to represent the intrinsic catalytic activity.[40] The ECSA normalized linear scan voltammetry (LSV) curves

(Fig. 5c) indicate that IronCE10s has the highest intrinsic catalytic activity. Moreover, the average overpotential required to reach 10 mA/cm^2-ecsa is below 300 mV for electrodes synthesized after 5 s or 10 s (Fig. 5d), especially for IronCE10s, which only requires 261.3 ± 6.2

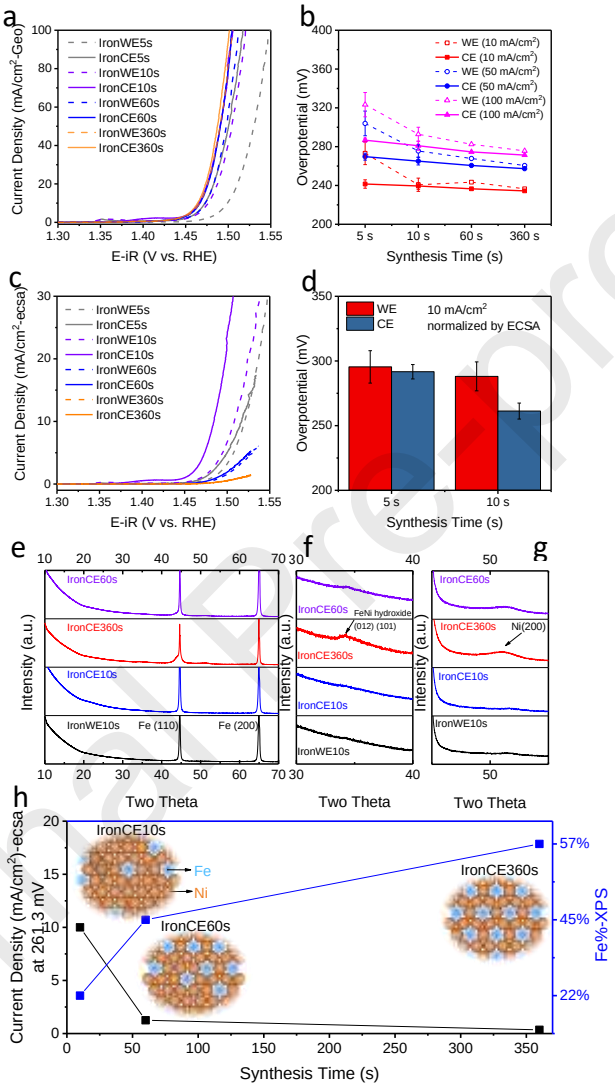

mV overpotential to reach 10 mA/cm^2-ecsa, such performance far exceeds many of the reported electrocatalysts (Table S1). In contrast, when the pulsed synthesis time was increased to 60 s and 360 s, the intrinsic catalytic activity actually tumbled significantly. For example, at the overpotential of 261.3 mV, IronCE60s and IronCE360s can only achieve 1.25 and 0.35 mA/cm^2-ecsa (Fig. 5c), which decreased around 87.5% and 96.5% compared with IronCE10s. These

results prove that longer synthesis time would endow the electrodes with lower specific catalytic activity.

Fig. 5. (a) LSV curves (1 mV/s) recorded in 1.0 M KOH of iron based electrodes synthesized by using 5, 10, 60 and 360 s. (b) Comparison of the overpotential required to catalyze 10, 50, 100 mA/cm^2 normalized by geometric areas for electrodes synthesized at various times. (c) Current density normalized by ECSA for electrodes synthesized at different times. (d) Comparison of overpotential required to reach 10 mA/cm^2 normalized by ECSA for IronWE/CE5s and IronWE/CE10s. (e) XRD patterns and (f) and (g), enlarged XRD curves for IronWE/CE10s, IronCE60s and IronCE360s. (h) The correlation of specific activity trend represented by the current density normalized with ECSA when overpotential = 261.3 mV and surface iron content measured by XPS for IronCE synthesized at 10, 60 and 360 s.

The structures of electrodes synthesized by various times were further investigated by XRD to understand the intrinsic catalytic activity difference. As shown in Fig. 5e, besides the two primary peaks at 44.7° and 65.0°, ascribed to iron substrate, there are no other major peaks. The enlarged area from 20° to 55° (Fig. 5f) displays two minor peaks at 34.2°, due to (012) / (101) of nickel/iron hydroxide, and 51.1°, indexed to metallic nickel for ironCE60s and IronCE360s. On the contrary, these peaks are almost negligible for IronWE10s and IronCE10s. The results suggest that after very short synthesis time, the $Fe_xNi_yO_zH_w$ metal hydroxide film on the surface predominantly contains highly disordered amorphous phase, which is beneficial for enhancing OER specific activity.[41-44] With longer continuous potential pulses, the crystallinity increases, causing diminished intrinsic catalytic activity. Besides the alteration of crystallinity degree, the surface Fe/Ni atomic ratios also changed with different synthesis time. Based on XPS analysis (Fig. S8 and Fig. 5g), the iron content increases with the increasing of synthesis time. After 360

s, the surface of IronCE360s becomes dominated with iron. When the synthesis time is only 10 s for IronCE10s, we propose that iron prefer to incorporate into nickel hydroxide phase at the defective sites or edge locations, while after prolonged synthesis time, iron can finally incorporate into the bulk phase of nickel hydroxide and therefore the percentage of iron content increases. The former structure is more active for OER compared with the latter one. On the basis of these results, we conclude that iron doped amorphous nickel hydroxide sites are the most active species for OER. This observation is similar with previous reports concluding that the location of iron in nickel hydroxide could impact OER performance and the surface iron plays more important role for OER catalysis.[45, 46]

Except for the catalytic activity normalized by ECSA, turn over frequency (TOF) was calculated to study the intrinsic catalytic activity precisely (Fig. 6). For IronWE/CE5s and IronWE/CE10s, TOF results calculated based on total transition metal hydroxides indicate that IronCE10s has the highest catalytic activity of 0.195 s^{-1} at 300 mV overpotential. This represents the lower limit of TOF as not all the transition metal sites are accessible or active. When TOF is calculated only based on surface electrochemically accessible transition metal sites, the TOF of IronCE10s is further improved to 0.429 s^{-1}, which is comparable to many state-of-the-art OER electrocatalysts (Table S2). Of note, the TOF of IronWE is smaller than IronCE, and the gap is larger in the case of TOF_{all} compared with $TOF_{surface}$, this is because there's higher portion of non-accesssible transition metal in IronWE, and the overall catalytic activity is largely dependent on how many of the active catalytic sites are accessible on the surface.

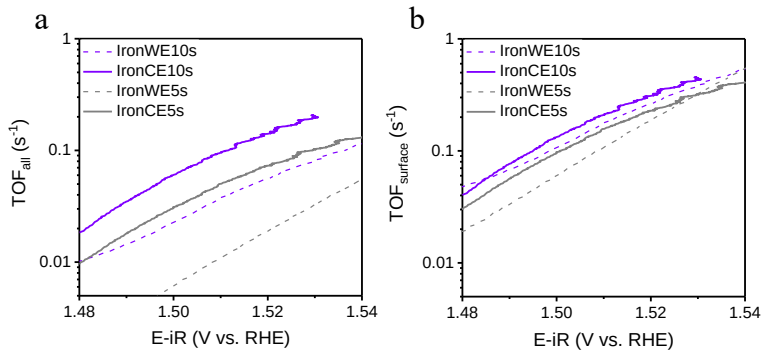

Fig. 6. Comparison of TOF for IronWE/CE10s and IronWE/CE5s based on total number the deposited iron + nickel (a) and based on surface electrochemically accessible transition metal sites.

3.3. Influence of Pulsed Potential on OER Activity

To further investigate the influence of potential values on the catalytic activity of as-synthesized iron-based electrodes, apart from the electrodes synthesized under the pulsed potential of ± 2.4 V, several electrodes were synthesized in a two-electrode setup under a series of potential pulses, namely, ± 0.4, ± 0.8, ± 1.2, ± 1.6, ± 2.0 and ± 4.0 V. As shown in Fig. 7a and 7b, the anodic current values become higher when the potential values increase, and the passed charges also have positive relationship with the applied potential values. The surface nickel loading also increased from ± 0.4 to ± 2.4 V and then reached a steady state (Fig. 7c). The catalytic activities of these electrodes were measured in 1.0 M KOH and the results confirmed that at about ± 2.4 V potential value, the performance reached a maximun point for both IronWE and IronCE (Fig. S9 and Fig. 7d). The above findings indicate that, in order to synthesize active water oxidation electrodes on both anodic side and cathodic side, pulsed potential at around ± 2.4 V is the optimized condition.

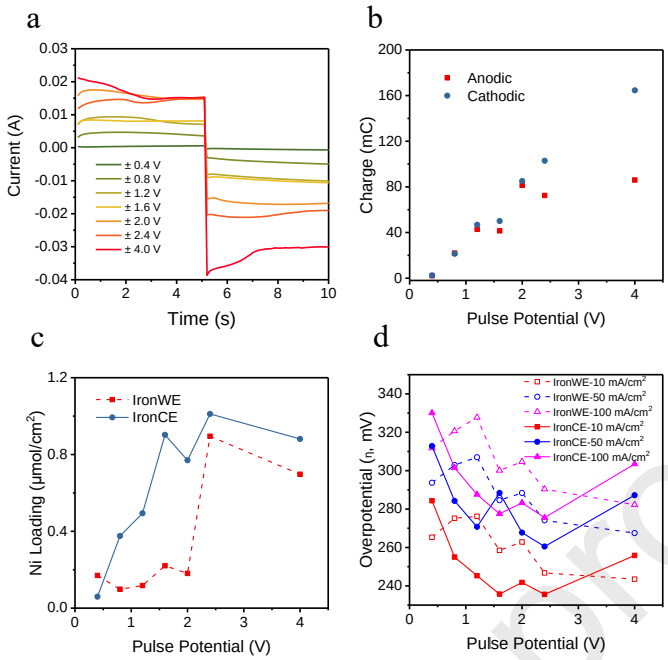

Fig. 7. (a) The current-time curve recorded over the course of two-electrode pulsed synthesis under various potential values. (b) The corresponding anodic/cathodic charge integrated from (a). (c) The electrochemically accessible nickel content obtained from integration of Ni^{2+}/Ni^{3+} reduction peaks. (d) Comparison of overpotential required to achieve 10, 50 and 100 mA/cm^2 OER catalytic current density for electrodes synthesized at different potentials.

3.4. Study of OER Stability

In order to check the stability of the electrodes, an accelerated method was used. The potential required to reach 100 mA/cm^2 current density was monitored in 1.0 M KOH for one hour, then the electrode was rinsed with ultrapure water to remove the electrolyte solution and put in 95% ethanol for 10 minutes' ultrasonication. Subsequently, the electrode was connected in a three-electrode cell again and the potential to catalyze OER at 100 mA/cm^2 was monitored for another hour. This process was repeated until 20 hour stability data was collected. As revealed in Fig. 8a and 8b, IronWE10s and IronCE10s can still catalyze OER, even after consecutive ultrasonic treatment. From the first hour to last hour, the potential shifted 25 and 51 mV for IronWE10s and

IronCE10s, respectively, indicating that the electrode can tolerate ultrasonication and the majority of active catalysts remained on the surface. This is further verified by SEM images and elemental mapping results of IronWE10s and IronCE10s measured after the stability test (Fig. 8cdef). Nanosheet arrays were still visible on both electrodes, and the surface was composed of iron, nickel and oxygen elements. However, the overall morphology and elemental distribution seems different compared with the observation before OER test as shown in Fig. 4, suggesting that there's structure reconstruction during OER. Similar morphology changes of $Ni(OH)_2$ and $Ni_{0.75}Fe_{0.25}(OH)_2$ were reported previously.[34] During the pulsed potential synthesis, the substrate iron elements actually participate in the formation of active catalyst, therefore, the new catalyst coating has strong affinity with the substrate, which renders the electrode with excellent stability. It's should be noted that without ultrasonic treatment, the potential kept relatively stable for both IronWE10s and IronCE10s (Fig. 8a and 8b).

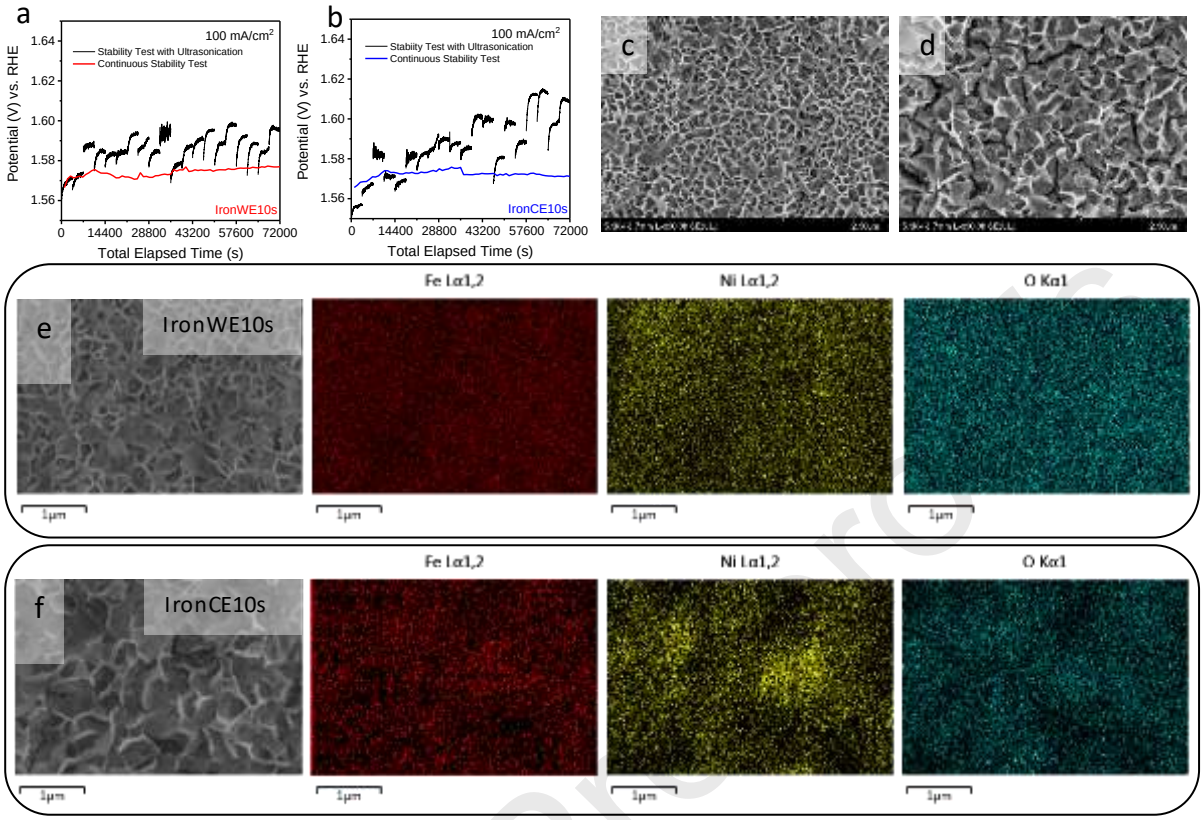

Fig. 8. Chronopotentiometric curve of (a) IronWE10s and (b) IronCE10s under continuous measurement or with 10 min ultrasonication between each segments. The SEM images of (c) IronWE10s and (d) IronCE10s after stability test with repeated ultrasonication. The elemental mapping of Fe, Ni, O for (e) IronWE10s and (f) IronCE10s after OER durability evaluation with repeated ultrasonication.

3.5. Scalable Synthesis of OER Electrodes

Based on above data, we have developed a method to synthesize two water oxidation electrodes, namely IronWE10s and IronCE10s, in merely 10 s, and both electrodes exhibit excellent water oxidation catalytic activity and stability. However, for large scale practical applications, it's appealing to synthesize a number of electrodes in short time. Inspired by the concept to synthesize two water oxidation electrodes simultaneously, two additional setups were devised and built to prepare more water oxidation electrodes at the same time. First we prepared

four electrodes by connecting 4 iron plates in parallel, two of them were connected with WE cable of potentiastat, another two were connected with RE+CE cable of potentiastat. By applying a pulsed potential of + 2.4 V (5 s) and – 2.4 V (5 s), four electrodes were fabricated in 10 s, which reduces the synthesis time to 2.5 s per electrode. The OER catalytic activity of these four electrodes were evaluated in 1.0 M KOH solution, and the LSV curves confirmed that they all had high catalytic activity (Fig. 9a), with the overpotential of 276.4, 286.2, 273.4 and 291.2 mV to reach 100 mA/cm^2 current density for 4-1CE, 4-2WE, 4-3CE and 4-4 WE, respectively. These overpotential values are roughly comparable with IronWE10s and IronCE10s, which require 292.8 ± 3.9 and 280.9 ± 7.2 mV to achieve the same 100 mA/cm^2 current density. The setup was further amplified to synthesize 10 water oxidation electrodes (Fig. S10). By using the same pulsed potential method, 10 water oxidation electrodes were synthesized in merely 10 s. During the course of synthesis, in the first 5 s with + 2.4 V applied on WE, the bubble generation due to hydrogen evolution was clearly observed on the 5 iron plates connected with CE+RE cable. Conversely, in the next 5 s, when – 2.4 V is applied on WE, the bubbles were seen on the other 5 iron plates connected with WE cable (See supporting video for more information). The LSV curves confirm that these 10 electrodes have close catalytic activities for OER (Fig. 9b), similar with above observation, the catalytic performance of IronCE generally surpass that of IronWE. This is due to the higher amount of active catalyst loading as confirmed by the electrochemically accessible nickel loading extrapolated from integration of Ni^{2+}/Ni^{3+} reduction peak in CV curves (Fig. 9c). The catalytic activities of these 10 electrodes were further compared by current density normalized with ECSA (Fig. S11) and all of them can reach 10 mA/cm^2-ecsa at the overpotential below 280 mV. The results are consistent with the two electrode setup. With this ten-electrode setup, it's doable to synthesize up to 10 electrodes in 10 s, the cycle time is reduced to merely 1 s per electrode. What is more attractive is that this proof of concept can be further extended to

synthesize a large number of water oxidation electrodes and lower the synthesis time below 1 s per electrode.

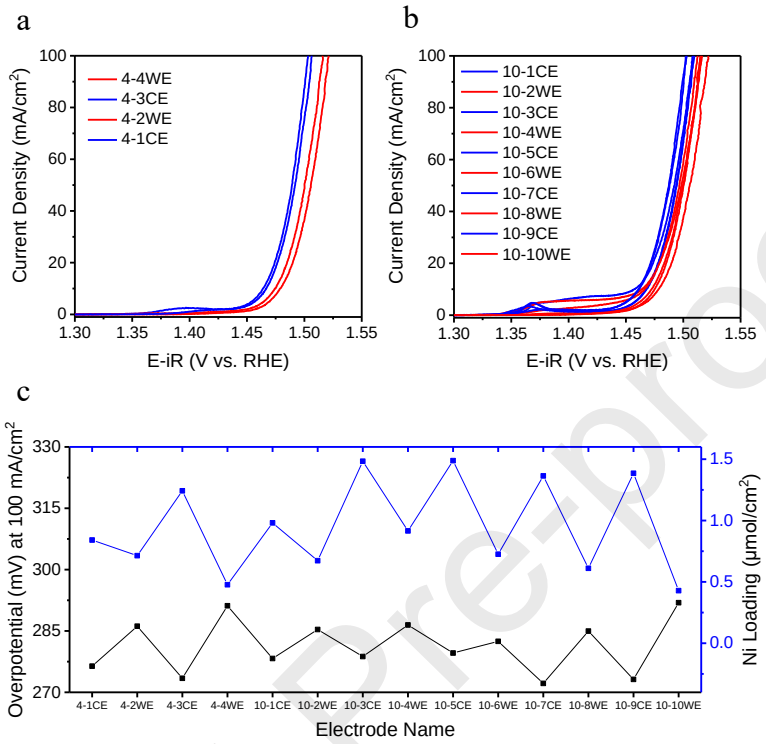

Fig. 9. LSV curves (1 mV/s) of iron based electrodes synthesized by using (a) two-electrode setup and (b) ten-electrode setup. (c) The comparison of overpotential at 100 mA/cm^2 and nickel loading for electrodes synthesized from scaled setup.

Besides parallel synthesis, we also investigated the possibility to synthesize larger porous electrode by pulsed potential method. Iron plate was punched with round holes and used as substrate for the synthesis as shown in Fig. S12ab. ± 2.4 V pulsed potential was applied between two iron nets for six loops (Fig. S13a). After the synthesis, the electrode was cut into small one to measure the OER catalytic activity at four different locations from each side (Fig. S12c). They have relatively similar catalytic activities as confirmed by the LSV curves (Fig. S13b), suggesting that the quality of the electrode is uniform. The OER activities on iron nets are

slightly lower than electrodes synthesized from smaller sized iron plate (Fig. S13c), which could be related with the presence of higher percentage of edge areas on smaller iron plate. At least this indicates that the concept of pulsed synthesis via two electrodes set up is possible to further scale up, future work should be focused on optimizing parameters of synthesis process to synthesize even larger electrode for practical application.

4. Conclusions

In summary, we have developed a new method to synthesize active water oxidation electrodes at ambient room temperature, by applying a pulsed potential between two iron strips in $NiSO_4$ solution for just 10 s. As both iron and $NiSO_4$ reagents are readily available materials, the described ultrafast method should offer a scalable route to synthesize efficient water oxidation electrodes in large scale. The resulting two water oxidation electrodes can catalyze OER with high catalytic activity–requires 240.7±6.8 mV and 239.5±3.4 mV to reach 10 mA/cm^2 geometric current density, and durable to catalyze OER even after repeated ultrasonication treatment. Considering both the synthesis time and catalytic performance, the IronWE10s and IronCE10s are among the best materials reported to date. Thanks to the presence of highly disordered amorphous structural motifs, IronWE10s and IronCE10s requires less than 300 mV overpotential to reach 10 mA/cm^2 current density normalized by ECSA, which is significantly better than other reported materials. In addition, the TOF at 300 mV is comparable to several state-of-the-art materials.

Acknowledgements

We thank Shenzhen Polytechnic for the support of this work.

REFERENCES

[1] R. Gao, D. Yan, Recent Development of Ni/Fe‐Based Micro/Nanostructures toward Photo/Electrochemical Water Oxidation, Adv.Energy Mater., 10 (2020) 1900954.
[2] Z.P. Wu, X.F. Lu, S.Q. Zang, X.W. Lou, Non‐Noble‐Metal‐Based Electrocatalysts toward the Oxygen Evolution Reaction, Adv.Funct. Mater., 30 (2020) 1910274.
[3] M.S. Burke, L.J. Enman, A.S. Batchellor, S. Zou, S.W. Boettcher, Oxygen Evolution Reaction Electrocatalysis on Transition Metal Oxides and (Oxy)hydroxides: Activity Trends and Design Principles, Chem. Mater., 27 (2015) 7549-7558.
[4] L. Lei, D. Huang, C. Zhou, S. Chen, X. Yan, Z. Li, W. Wang, Demystifying the active roles of NiFe-based oxides/(oxy)hydroxides for electrochemical water splitting under alkaline conditions, Coord. Chem. Rev., 408 (2020) 213177.
[5] J. Song, C. Wei, Z.F. Huang, C. Liu, L. Zeng, X. Wang, Z.J. Xu, A review on fundamentals for designing oxygen evolution electrocatalysts, Chem. Soc. Rev., 49 (2020) 2196-2214.
[6] T. Meng, Q. Li, M. Yan, D. Wang, L. Fan, X. Liu, Z. Xing, X. Yang, Electrochemically induced in-situ surface self-reconstruction on Ni, Fe, Zn ternary-metal hydroxides towards the oxygen-evolution performance, Chem. Eng. J., 410 (2021) 128331.
[7] Z. Liu, B. Tang, X. Gu, H. Liu, L. Feng, Selective structure transformation for NiFe/$NiFe_2O_4$ embedded porous nitrogen-doped carbon nanosphere with improved oxygen evolution reaction activity, Chem. Eng. J., 395 (2020) 125170.
[8] S. Anantharaj, S. Kundu, S. Noda, "The Fe Effect": A review unveiling the critical roles of Fe in enhancing OER activity of Ni and Co based catalysts, Nano Energy, 80 (2021) 105514.
[9] Z. Wang, J. Zhang, Q. Yu, H. Yang, X. Chen, X. Yuan, K. Huang, X. Xiong, Synthesis of 3D CoO nanowires supported NiFe layered double hydroxide using an atmospheric pressure microplasma for high-performance oxygen evolution reaction, Chem. Eng. J., 410 (2021) 128366.
[10] L. Wu, L. Yu, F. Zhang, D. Wang, D. Luo, S. Song, C. Yuan, A. Karim, S. Chen, Z. Ren, Facile synthesis of nanoparticle-stacked tungsten-doped nickel iron layered double hydroxide nanosheets for boosting oxygen evolution reaction, J. Mater. Chem. A, 8 (2020) 8096-8103.
[11] A. Karmakar, K. Karthick, S.S. Sankar, S. Kumaravel, R. Madhu, S. Kundu, A vast exploration of improvising synthetic strategies for enhancing the OER kinetics of LDH structures: a review, J. Mater. Chem. A, 9 (2021) 1314-1352.
[12] F. Bu, W. Chen, M.F. Aly Aboud, I. Shakir, J. Gu, Y. Xu, Microwave-assisted ultrafast synthesis of adjustable bimetal phosphide/graphene heterostructures from MOFs for efficient electrochemical water splitting, J. Mater. Chem. A, 7 (2019) 14526-14535.
[13] X. Zou, Y. Liu, G.D. Li, Y. Wu, D.P. Liu, W. Li, H.W. Li, D. Wang, Y. Zhang, X. Zou, Ultrafast Formation of Amorphous Bimetallic Hydroxide Films on 3D Conductive Sulfide Nanoarrays for Large-Current-Density Oxygen Evolution Electrocatalysis, Adv. Mater., 29 (2017) 1700404.
[14] L. Yu, L. Wu, B. McElhenny, S. Song, D. Luo, F. Zhang, Y. Yu, S. Chen, Z. Ren, Ultrafast room-temperature synthesis of porous S-doped Ni/Fe (oxy)hydroxide electrodes for oxygen evolution catalysis in seawater splitting, Energy Environ. Sci., 13 (2020) 3439-3446.
[15] X. Yang, Q.-Q. Chen, C.-J. Wang, C.-C. Hou, Y. Chen, Substrate participation ultrafast synthesis of amorphous NiFe nanosheets on iron foam at room temperature toward highly efficient oxygen evolution reaction, J. Energy Chem., 35 (2019) 197-203.
[16] G. Ren, Q. Hao, J. Mao, L. Liang, H. Liu, C. Liu, J. Zhang, Ultrafast fabrication of nickel sulfide film on Ni foam for efficient overall water splitting, Nanoscale, 10 (2018) 17347-17353.

[17] Y. Chen, S. Xu, S. Zhu, R.J. Jacob, G. Pastel, Y. Wang, Y. Li, J. Dai, F. Chen, H. Xie, B. Liu, Y. Yao, L.G. Salamanca-Riba, M.R. Zachariah, T. Li, L. Hu, Millisecond synthesis of CoS nanoparticles for highly efficient overall water splitting, Nano Res., 12 (2019) 2259-2267.
[18] Z. Li, M. Shao, H. An, Z. Wang, S. Xu, M. Wei, D.G. Evans, X. Duan, Fast electrosynthesis of Fe-containing layered double hydroxide arrays toward highly efficient electrocatalytic oxidation reactions, Chem. Sci., 6 (2015) 6624-6631.
[19] A.S. Batchellor, S.W. Boettcher, Pulse-Electrodeposited Ni–Fe (Oxy)hydroxide Oxygen Evolution Electrocatalysts with High Geometric and Intrinsic Activities at Large Mass Loadings, ACS Catal., 5 (2015) 6680-6689.
[20] Y. Li, X. Zhou, W. Qi, H. Xie, K. Yin, Y. Tong, J. He, S. Gong, Z. Li, Ultrafast fabrication of Cu oxide micro/nano-structures via laser ablation to promote oxygen evolution reaction, Chem. Eng. J., 383 (2020) 123086.
[21] H.S. Jadhav, A.C. Lim, A. Roy, J.G. Seo, Room-Temperature Ultrafast Synthesis of NiCo-Layered Double Hydroxide as an Excellent Electrocatalyst for Water Oxidation, ChemistrySelect, 4 (2019) 2409-2415.
[22] Y.K. Kim, J.H. Kim, Y.H. Jo, J.S. Lee, Precipitating Metal Nitrate Deposition of Amorphous Metal Oxyhydroxide Electrodes Containing Ni, Fe, and Co for Electrocatalytic Water Oxidation, ACS Catal., 9 (2019) 9650-9662.
[23] Q. Liu, H. Zhang, J. Xu, L. Wei, Q. Liu, X. Kong, Facile Preparation of Amorphous Fe-Co-Ni Hydroxide Arrays: A Highly Efficient Integrated Electrode for Water Oxidation, Inorg. Chem., 57 (2018) 15610-15617.
[24] X. Tian, Y. Liu, D. Xiao, J. Sun, Ultrafast and large scale preparation of superior catalyst for oxygen evolution reaction, J. Power Sources, 365 (2017) 320-326.
[25] F. Guo, Y. Wu, H. Chen, Y. Liu, L. Yang, X. Ai, X. Zou, High-performance oxygen evolution electrocatalysis by boronized metal sheets with self-functionalized surfaces, Energy Environ. Sci., 12 (2019) 684-692.
[26] Y. Liu, X. Liang, L. Gu, Y. Zhang, G.D. Li, X. Zou, J.S. Chen, Corrosion engineering towards efficient oxygen evolution electrodes with stable catalytic activity for over 6000 hours, Nat. Commun., 9 (2018) 2609.
[27] B. Chen, Z. Zhang, S. Kim, M. Baek, D. Kim, K. Yong, A biomimetic nanoleaf electrocatalyst for robust oxygen evolution reaction, Appl. Catal. B, 259 (2019) 118017.
[28] L. Huang, D. Chen, G. Luo, Y.R. Lu, C. Chen, Y. Zou, C.L. Dong, Y. Li, S. Wang, Zirconium‐Regulation‐Induced Bifunctionality in 3D Cobalt‐Iron Oxide Nanosheets for Overall Water Splitting, Adv. Mater., 31 (2019) 1901439.
[29] Y. Shi, Y. Yu, Y. Liang, Y. Du, B. Zhang, In Situ Electrochemical Conversion of an Ultrathin Tannin Nickel Iron Complex Film as an Efficient Oxygen Evolution Reaction Electrocatalyst, Angew. Chem. Int. Ed., 58 (2019) 3769-3773.
[30] Z. Zhang, X. Li, C. Zhong, N. Zhao, Y. Deng, X. Han, W. Hu, Spontaneous Synthesis of Silver-Nanoparticle-Decorated Transition-Metal Hydroxides for Enhanced Oxygen Evolution Reaction, Angew. Chem. Int. Ed., 59 (2020) 7245-7250.
[31] C. Wang, H. Yang, Y. Zhang, Q. Wang, NiFe Alloy Nanoparticles with hcp Crystal Structure Stimulate Superior Oxygen Evolution Reaction Electrocatalytic Activity, Angew. Chem. Int. Ed., 58 (2019) 6099-6103.
[32] S. Liu, J. Zhang, H. Wang, T. Asefa, X. Huang, A Facile Route to Efficient Water Oxidation Electrodes via Electrochemical Activation of Iron in Nickel Sulfate Solution, ACS Sustainable Chem. Eng., 8 (2020) 15550-15559.
[33] B. Zhang, L. Wang, Z. Cao, S.M. Kozlov, F.P. García de Arquer, C.T. Dinh, J. Li, Z. Wang, X. Zheng, L. Zhang, Y. Wen, O. Voznyy, R. Comin, P. De Luna, T. Regier, W. Bi, E.E. Alp, C.-

W. Pao, L. Zheng, Y. Hu, Y. Ji, Y. Li, Y. Zhang, L. Cavallo, H. Peng, E.H. Sargent, High-valence metals improve oxygen evolution reaction performance by modulating 3d metal oxidation cycle energetics, Nat. Catal., 3 (2020) 985–992.
[34] L. Trotochaud, S.L. Young, J.K. Ranney, S.W. Boettcher, Nickel–Iron Oxyhydroxide Oxygen-Evolution Electrocatalysts: The Role of Intentional and Incidental Iron Incorporation, J. Am. Chem. Soc., 136 (2014) 6744-6753.
[35] C. Roy, B. Sebok, S.B. Scott, E.M. Fiordaliso, J.E. Sørensen, A. Bodin, D.B. Trimarco, C.D. Damsgaard, P.C.K. Vesborg, O. Hansen, I.E.L. Stephens, J. Kibsgaard, I. Chorkendorff, Impact of nanoparticle size and lattice oxygen on water oxidation on NiFeOxHy, Nat. Catal., 1 (2018) 820-829.
[36] J. Chen, F. Zheng, S.-J. Zhang, A. Fisher, Y. Zhou, Z. Wang, Y. Li, B.-B. Xu, J.-T. Li, S.-G. Sun, Interfacial Interaction between FeOOH and Ni–Fe LDH to Modulate the Local Electronic Structure for Enhanced OER Electrocatalysis, ACS Catal., 8 (2018) 11342-11351.
[37] H. Lee, X. Wu, Q. Ye, X. Wu, X. Wang, Y. Zhao, L. Sun, Hierarchical CoS2/Ni3S2/CoNiOx nanorods with favorable stability at 1 A cm(-2) for electrocatalytic water oxidation, Chem. Commun., 55 (2019) 1564-1567.
[38] L. Yu, H. Zhou, J. Sun, F. Qin, F. Yu, J. Bao, Y. Yu, S. Chen, Z. Ren, Cu nanowires shelled with NiFe layered double hydroxide nanosheets as bifunctional electrocatalysts for overall water splitting, Energy Environ. Sci., 10 (2017) 1820-1827.
[39] J. Zhang, S. Liu, H. Wang, Q. Xia, X. Huang, Polypyrrole assisted synthesis of nanosized iridium oxide for oxygen evolution reaction in acidic medium, Int. J. Hydrogen Energy, 45 (2020) 33491-33499.
[40] J. Li, H. Chen, Y. Liu, R. Gao, X. Zou, In situ structural evolution of a nickel boride catalyst: synergistic geometric and electronic optimization for the oxygen evolution reaction, J. Mater. Chem. A, 7 (2019) 5288-5294.
[41] W. Cai, R. Chen, H. Yang, H.B. Tao, H.Y. Wang, J. Gao, W. Liu, S. Liu, S.F. Hung, B. Liu, Amorphous versus Crystalline in Water Oxidation Catalysis: A Case Study of NiFe Alloy, Nano Lett., 20 (2020) 4278-4285.
[42] J. Nai, H. Yin, T. You, L. Zheng, J. Zhang, P. Wang, Z. Jin, Y. Tian, J. Liu, Z. Tang, L. Guo, Efficient Electrocatalytic Water Oxidation by Using Amorphous Ni-Co Double Hydroxides Nanocages, Adv. Energy Mater., 5 (2015) 1401880.
[43] R.D. Smith, M.S. Prevot, R.D. Fagan, Z. Zhang, P.A. Sedach, M.K. Siu, S. Trudel, C.P. Berlinguette, Photochemical route for accessing amorphous metal oxide materials for water oxidation catalysis, Science, 340 (2013) 60-63.
[44] S. Li, X. Yang, S. Yang, Q. Gao, S. Zhang, X. Yu, Y. Fang, S. Yang, X. Cai, An amorphous trimetallic (Ni–Co–Fe) hydroxide-sheathed 3D bifunctional electrode for superior oxygen evolution and high-performance cable-type flexible zinc–air batteries, J. Mater. Chem. A, 8 (2020) 5601-5611.
[45] M.B. Stevens, C.D.M. Trang, L.J. Enman, J. Deng, S.W. Boettcher, Reactive Fe-Sites in Ni/Fe (Oxy)hydroxide Are Responsible for Exceptional Oxygen Electrocatalysis Activity, J. Am. Chem. Soc., 139 (2017) 11361-11364.
[46] R. Wang, C. Wang, S. Yin, Y. Peng, J. Chen, Y. Deng, J. Li, Hierarchically devising NiFeOH catalyst with surface Fe active sites for efficient oxygen evolution reaction, Catal. Today, (2020).